



Thermal conductivity and interface thermal conductance of thin films in Li ion batteries



K. Jagannadham

Materials Science and Engineering, North Carolina State University, Raleigh, NC 27695, USA

HIGHLIGHTS

- Thermal conductivity and interface thermal conductance of thin films is determined.
- LIPON film is found to be a thermal barrier.
- Crystalline cathode and graphene anode films are effective heat spreaders.
- Interface thermal conductance between films is found to be a critical parameter.

ARTICLE INFO

Article history:

Received 13 June 2016

Received in revised form

22 July 2016

Accepted 25 July 2016

Keywords:

LIPON

LiNiMnO

Graphene

Thermal conductivity

Interface thermal conductance

ABSTRACT

Laser physical vapor deposition is used to deposit thin films of lithium phosphorous oxynitride in nitrogen and lithium nickel manganese oxide in oxygen ambient on Si substrate. LIPON film is also deposited on LiNiMnO film that is deposited on Si. Graphene films consisting of graphene platelets are deposited on Si substrate from a suspension in isopropyl alcohol. Li-graphene films are obtained after Li adsorption by immersion in LiCl solution and further drying. Transient thermo reflectance signal is used to determine the cross-plane thermal conductivity of different layers and interface thermal conductance of the interfaces. The results show that LIPON film with lower thermal conductivity is a thermal barrier. The interface thermal conductance between LIPON and Au or Si is found to be very low. Thermal conductivity of LiNiMnO is found to be reasonably high so that it is not a barrier to thermal transport. Film with graphene platelets shows a higher value and Li adsorbed graphene film shows a much higher value of cross-plane thermal conductivity. The value of interface thermal conductance between graphene and Au or Si (100) substrate is also much lower. The implications of the results for the thermal transport in thin film Li batteries are discussed.

© 2016 Elsevier B.V. All rights reserved.

1. Introduction

The performance of batteries is a function of temperature as the thermal effects [1] include capacity or power fade, self-discharge, thermal runaway and electrical balance in assembly of batteries. Many investigations have been carried out [2–5] on the thermal conductivity of positive and negative electrode materials in large Li-ion batteries used for electric vehicle applications. Fundamental study of lower thermal conductivity of Si nanowires upon Li ion insertion showed phonons are scattered by phonon rattling effect [6]. Thermal conductivity improvement by use of carbon nanotube layers [7] with embedded γ -Fe₂O₃ particles has been reported. In the present work, we considered the different components of Li-ion

thin film batteries and evaluated the thermal conductivity and interface thermal conductance to provide a valuable insight into the critical parameters that control the thermal energy dissipation. The components include thin films of positive electrode of LiNi_{0.5}Mn_{1.5}O₄ (LiNiMnO), negative electrode of graphene with adsorbed Li ions, and the solid electrolyte of lithium phosphorous oxynitride (LIPON). The choice of the thin films studied in the present work is based upon the high voltage at which LiNiMnO (4.8 V) can be operated for high capacity batteries [8–10], the stability of LIPON upon charge and discharge cycling [11] (5.5 V) and the high capacity of lithium-graphene [12,13] or Li–Si anodes [14]. In order to determine the effect of Li adsorption on graphene platelets, thermal conductivity of graphene thin film consisting of graphene platelets has also been investigated in the absence of Li. The interface thermal conductance between the thin films and Si is evaluated as Si is considered as a high capacity anode material. The

E-mail address: jag_kasichainula@ncsu.edu.

importance of microstructure and interface roughness of the components for the thermal energy dissipation in the thin film battery is emphasized.

2. Experimental procedure

2.1. 1 preparation of the films

Thin films of LiNiMnO and LIPON were deposited on Si (100) substrates using laser physical vapor deposition (LPVD). Composite layered film of LIPON on LiNiMnO was also deposited on Si substrate following the same procedure. Target materials of LiNiMnO and Li_3PO_4 were used in the deposition. Nd-YAG laser source in the fourth harmonic ($\lambda = 266$ nm) with pulse duration of 6 ns, energy per pulse of 210 mJ and repetition rate of 10 Hz was used for laser ablation. LiNiMnO film was deposited at 550 °C for 1 h in oxygen partial pressure of 200 mTorr (26.64 Pa). LIPON film was deposited at 250 °C for 1.5 h in nitrogen partial pressure of 200 mTorr (26.64 Pa). LiNiMnO was deposited first on Si for 1 h in oxygen and LIPON was deposited on the top for 1.5 h in nitrogen for the composite layered film. The Si substrate was cleaned in acetone followed by native oxide etch in 45% HF for 1 min and rinse in deionized water before loading onto substrate holder in the vacuum chamber. Pre-deposition vacuum of 1.0×10^{-6} Torr (133.3×10^{-6} Pa) was achieved by means of a turbo pump backed by a mechanical pump. The substrate was heated to the deposition temperature by a resistance heater and monitored with a thermocouple in contact with the substrate holder.

Graphene films were deposited on Si substrate from a suspension of graphene platelets in isopropyl alcohol that was prepared separately. The details of graphene synthesis were described at length in our previous work [15]. Si substrates prepared using the procedure described above were used. Graphene platelet suspension in isopropyl alcohol was collected through a 3 mm diameter glass tube and dispersed on the Si substrate. The deposition was continued until the thickness of the film was close to 4 μm . The graphene film was smoothened with a sharp straight edge and dried. The film was not pressed.

Graphene films were lithiated by sonicating in LiCl solution [16]. LiCl solution was prepared by reacting Li metal with 10 mL of concentrated HCl. The addition of Li foil to the solution mixture was continued until no further reaction of Li was observed. Graphene platelets prepared by drying from the alcohol suspension were dispersed in 10 mL LiCl solution and sonicated for 24 h at low power. Sonication was repeated three times with separation of 24 h. The paste of graphene platelets in LiCl was collected and dispersed on Si substrate to achieve the desired thickness. The film was smoothened with a sharp and straight edge and dried on a hot plate kept at 150 °C for several hours to remove the Cl and was subsequently retained in a desiccator. X-ray diffraction from the film showed the elimination of hygroscopic LiCl upon repeated drying. Further characterization was carried out using energy dispersive spectrometry (EDS) to determine the absence of Cl in the film.

The films were characterized by X-ray diffraction for crystallinity, scanning electron microscopy (SEM) for microstructure and morphology, energy dispersive spectroscopy (EDS) for presence of impurities and transient thermoreflectance (TTR) for thermal conductivity and interface thermal conductance.

2.2. Measurement of thermal transport properties

The value of thermal conductivity and interface thermal conductance was determined by transient thermoreflectance (TTR) measurements. Au transducer film was deposited by LPVD on the surface of the film for purposes of collecting the TTR signal. A

schematic of the sample structure used for the TTR signal measurement is shown in Fig. 1 for LiNiMnO film on Si and the same is valid for the other films. The details of the TTR setup are provided in our previous work [17] and reference [18] and not repeated here for brevity. Briefly, pump laser beam of wave length 532 nm from second harmonic Nd-YAG laser at low pulse energy was used to instantaneously heat the substrate at repetition rate of 10 Hz and the pulse duration was recorded. A continuous laser probe beam of wave length 650 nm from a laser diode was used to measure the TTR signal. The power of the probe laser was adjusted between 10 and 15 mW to improve the TTR signal without heating the sample surface. Both the beams were focused on to the Au transducer film on the sample through a microscope objective. The reflected light from the sample was collected into a Si photodiode with response time of 1 ns after filtering the Nd-YAG laser light. The output from the photodiode is amplified through a preamplifier and recorded digitally using an oscilloscope. The oscilloscope signal was triggered using the output from a second Si photodiode that was used to detect the pump beam pulse before it was incident on the sample surface.

3. Experimental results

3.1. X-ray diffraction

X-ray diffraction peak profile from LiNiMnO film was collected using a Rigaku instrument in the coupled θ - 2θ configuration using Cu K_α radiation and the profile is shown in Fig. 2(a). The peaks are identified from JCPD 32.581 and reference [10]. The LIPON film on Si was amorphous and did not exhibit any peaks. The profile from graphene film on Si is shown in Fig. 2(b).

3.2. Scanning electron microscopy (SEM) and energy dispersive spectrometry (EDS)

The samples were examined in the FEI Verios 460L high resolution field emission scanning electron microscope equipped with Oxford EDS detector with high count rate. Both the secondary electron and back scattering detectors were used to collect the images. SEM images of LiNiMnO film shown in Fig. 3(a) and (b) along with the EDS shown in Fig. 3(c) indicate that particulates from the laser generated plume are present. The circular dots are indicative of the molten droplets that are formed during laser ablation but solidified upon reaching the substrate. The absence of impurities in the film is inferred from EDS spectrum presented in Fig. 3(c).

SEM images of LIPON film presented in Fig. 4(a) and (b) along with the EDS shown in Fig. 4(c) again indicate the presence of particulates in the film. The sintered density of the Li_3PO_4 target is low, thus, allowing more particulate ejection from the target. The appearance of the dark particulates in the back scattering image that appear bright in the secondary electron image signifies that the average atomic number of elements in the particulates is low. Thus, the particulates are considered richer in Li and O than the film. SEM image from LIPON film deposited on LiNiMnO film on Si is



Fig. 1. Schematic illustration of geometry of laser incidence on the sample surface. For other samples, LiNiMnO is replaced by the other films. The two laser beams were focused to the same point although shown separate for clarity.

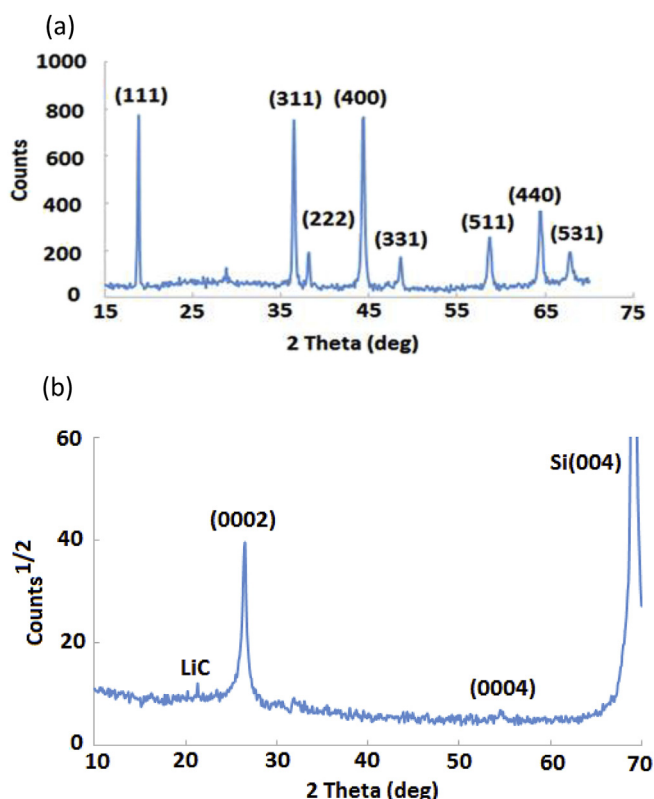


Fig. 2. (a). X-ray diffraction peak profile obtained from LiNiMnO film deposited on Si(100) substrate and indexed using JCPD 32–581. The peak at $2\theta = 67.7^\circ$ was identified to be (531) by others [8] although not listed in the JCPD 32–581. The unidentified peak at 28.6° was due to mounting clay on the stage. The Si (004) peak is suppressed by the high atomic number Ni and Mn in the film. (b). X-ray diffraction peak profile obtained from Li-graphene film on Si (100) substrate. The graphite peaks (0002) and (0004) are indexed. The small peak from LiC phase is not strong because both Li and C are elements with low atomic number and the fraction of LiC phase in the graphene film is very small.

presented in Fig. 5(a) and (b) from the secondary and backscattering modes, respectively. The sample was coated with Au film to obtain a better SEM image. LIPON film on the surface contained laser ablated particulates but otherwise the film is relatively smooth. The EDS spectrum, shown in Fig. 5(c) contained all the peaks expected including Ni, Mn, O, Si and Au. The signal from P that was present between Si and Au signal is over shadowed by the strong Au peak but the asymmetry of Au peak indicated the presence of P in the film.

SEM images from Li adsorbed graphene film, shown in Fig. 6(a) and (b), indicate that the surface is not very smooth. Strong C signal from graphene platelets is present in the EDS spectrum from the film, shown in Fig. 6(c). In addition, O signal is also present from formation of Li_2O when the film is heated to drive out the Cl. Au signal arises from the film deposited to improve the image. The weak Cu signal is thought to arise from an impurity in Li foil that is dissolved in HCl.

3.3. Transient thermoreflectance (TTR)

The normalized TTR signal from the different films on Si substrate is shown in Fig. 7(a)–(e). The wavy experimental result from all the films is a result of surface and interface roughness. The diameter of the pump laser beam is close to $300\ \mu\text{m}$ and that of the probe laser beam is $200\ \mu\text{m}$. The TTR signal is collected from the smooth Au surface. However, the interface roughness is a function

of the surface roughness of the film on which Au film was deposited. In particular, presence of larger size particulates in the LIPON film was responsible for a signal that exhibited higher waviness, as shown in Fig. 7(b). The larger value of the laser beam diameter included the effect of surface and interface roughness on the TTR signal.

3.4. Analysis of the TTR signal

The sample is divided into three regions for purposes of analysis, as shown in Fig. 1. Thermal diffusion is one-dimensional [15,18] as the diameter of the incident pump laser beam is much larger than the thermal diffusion depth into the sample. The diffusion equation [17–22] is solved numerically using finite difference method. The boundary conditions include the heat flux at the surface from the incident laser beam and at the interfaces [18]. The interface thermal conductance, h , at each interface is determined using flux $J = -h\ dT$ where dT is the temperature difference between the two adjacent regions. Detailed set of equations associated with the boundary conditions at each interface are presented in our previous work [17,19–22] and reference [18] and not repeated here for brevity. The value of interface thermal conductance at the first interface between Au transducer and the deposited film, either LiNiMnO or LIPON or Li-graphene or graphene is h_{12} and that between the film and the Si substrate is h_{23} . When the thermal conductivity of the film is very low such as in LIPON, the thermal diffusion depth is very small so that Si substrate and the interface between the film and the substrate are not important in the analysis.

The parameters used in the analysis included the thickness, heat capacity and thermal conductivity of each layer and the two values of interface thermal conductance. The thermal conductivity of the top Au film is measured separately on a sample deposited on Si from the measurement of electrical conductivity and use of Wiedemann-Franz law [23] and found to be $70\ \text{W m}^{-1}\text{K}^{-1}$. The heat capacity of Au is $2.3\ \text{MWm}^{-3}\text{K}^{-1}$. The thermal diffusion time through the thickness ($0.15\ \mu\text{m}$) of the Au transducer film is $0.4\ \text{ns}$. Therefore, thermal diffusion time in Au (region 1) is much smaller than in the film (region 2), K_2 , present on Si substrate and thus, the results are not significantly affected by the thickness of the Au film. The only parameters that were determined from the analysis were the thermal conductivity of the film (region 2) and the value of the interface thermal conductance of the two interfaces (h_{12} and h_{23}). The thickness of region 3, t_3 , is the value used in the analysis to simulate the results. A value of $t_3 = 8\ \mu\text{m}$ is sufficiently large that thermal diffusion occurs well into the substrate. However, t_3 is smaller when thermal diffusion is reduced. As mentioned previously, the thickness of region 3 was not important when the thermal conductivity of the film (region 2) is very low. The thermal conductivity and the heat capacity of Si was taken to be $150\ \text{W m}^{-1}\text{K}^{-1}$ and $1.65\ \text{MWm}^{-3}\text{K}^{-1}$, respectively. The heat capacity of graphene platelets is taken to be $1.6\ \text{MWm}^{-3}\text{K}^{-1}$ [19–22].

The normalized TTR signal was curve fitted with the values of the three parameters using least square curve fitting [24] to give R^2 value close to 0.995. The two regions of different slope and the middle region of each TTR signal, shown in Fig. 7(a)–(e), were useful to curve fit the TTR signal variation. Results of curve fitting for each sample, shown in Fig. 7(a)–(e), contain two curve fitted results in addition to the experimental results. The two curve fitted results are shown to illustrate the effect of an important parameter to achieve higher value of R^2 parameter. The time step was chosen as $0.05\ \text{ns}$ and the distance step was determined to satisfy the stability condition of the numerical solution [24]. The thickness of the film was sufficiently large to separate the two interfaces so that the thermal diffusion time in the film was large and the TTR signal was collected every nanosecond. The results of three parameters

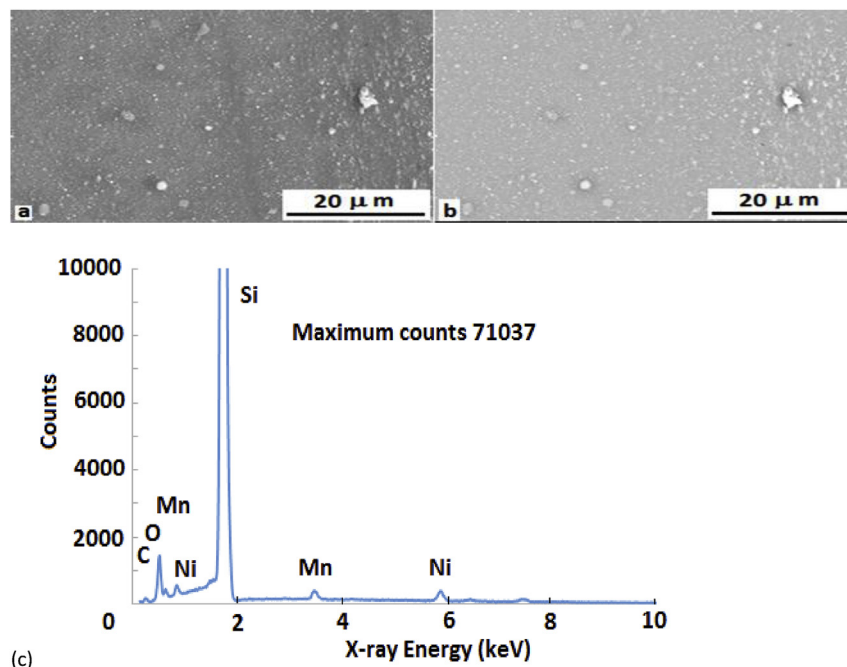


Fig. 3. (a) Secondary electron image and (b) backscattering image of the LiNiMnO film on Si substrate deposited by LPVD. The thickness of the film is measured to be 0.4 μm. (c) Energy dispersive spectrum collected from the LiNiMnO film on Si showing the presence of Ni, Mn and O in the film. The signal from C is thought to arise from hydrocarbons present on the surface in the SEM.

used in curve fitting for all the samples are shown Table 1. The error in the results of analysis that arises from thickness measurements and heat capacity is estimated to be ~10%, as shown in Table 1. The heat capacity of LiNiMnO is determined from Neumann-Kopp approximation [25] and found to be $3.0 \text{ MWm}^{-3}\text{K}^{-1}$ while that of LIPON is found to be $2.2 \text{ MWm}^{-3}\text{K}^{-1}$. Thickness of region 1 or Au layer (t_1) on all samples is 0.15 μm.

4. Discussion

The LiNiMnO film was crystalline and exhibited all the

characteristic peaks in the X-ray diffraction, shown in Fig. 2(a). SEM images, presented in Fig. 3(a) and (b), indicate a smooth film consisting of laser generated particulates. EDS results presented in Fig. 3(c) contains only peaks associated with Ni, Mn and O. LIPON film was amorphous and the SEM images in Fig. 4(a) and (b) contained larger particles that showed dark contrast in the backscattering image that indicates higher Li percentage and lower average atomic number. The nitrogen peak in EDS shown in Fig. 4(c) was weak although the deposition was carried out at 250 °C in higher nitrogen partial pressure of 200 mTorr (26.64 Pa). The O and P peaks were strong. Thus, incorporation of nitrogen into the LIPON

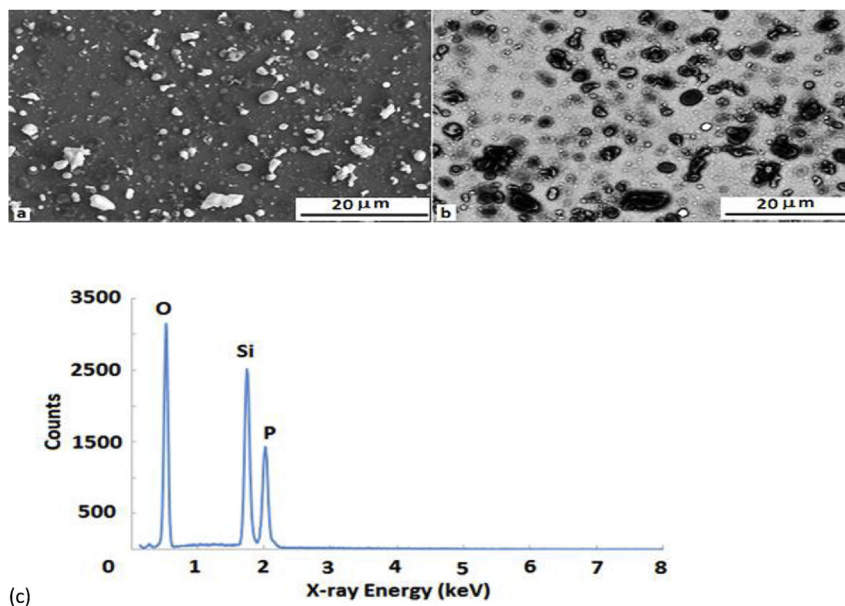


Fig. 4. (a) Secondary electron image and (b) backscattering image of the LIPON film on Si substrate deposited by LPVD. The thickness of the film is measured to be 0.4 μm. (c) Energy dispersive spectrum collected from the LIPON film on Si showing the presence of P and O in the film. The signal from N is very weak.

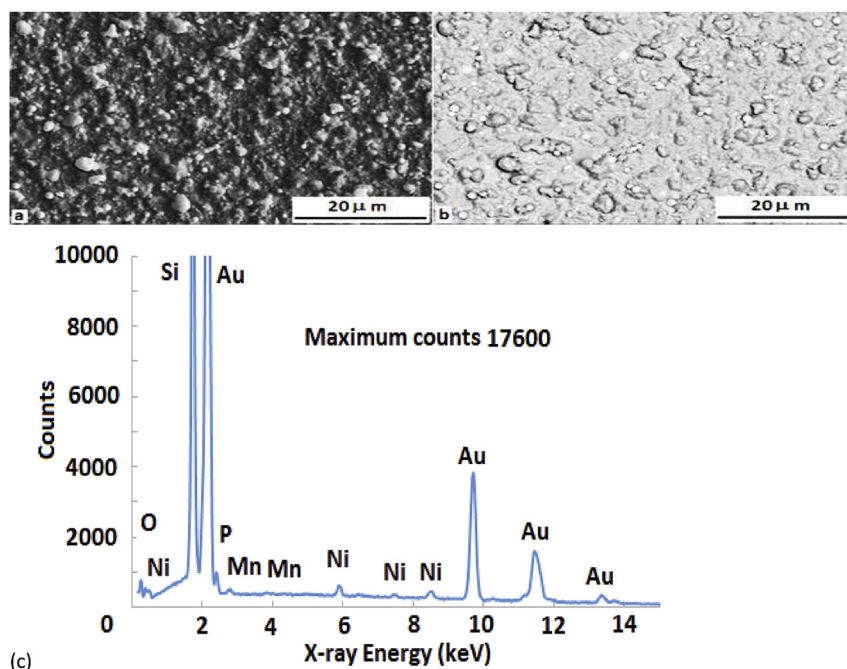


Fig. 5. (a) Secondary electron image and (b) backscattering image of the LiPON-LiNiMnO film on Si substrate deposited by LPVD. The thickness of the LiPON film is 0.4 μm and that of LiNiMnO film is 0.4 μm . (c) Energy dispersive spectrum collected from the LiPON-LiNiMnO film on Si showing the presence of Ni, Mn, P and O in the film. The signal from Au is from coating given to obtain better image. Signal from P is between Si and Au signals and it is determined by the asymmetry of the Au peak.

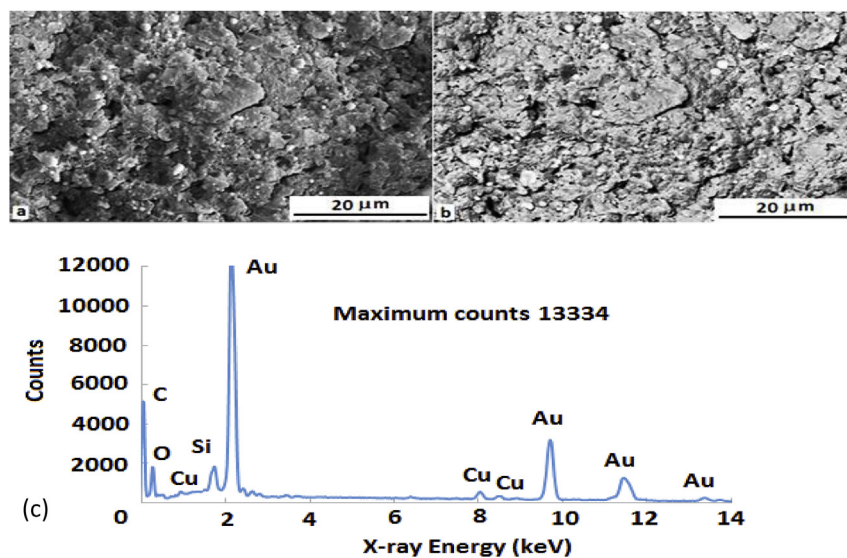


Fig. 6. (a) Secondary electron image and (b) backscattering image of the Li-graphene film on Si substrate. Au film of thickness 0.15 μm was deposited on the surface to get a better image of the morphology of the graphene platelets. The thickness of the Li-graphene film is measured to be 4.0 μm . (c) Energy dispersive spectrum collected from the Li-graphene film on Si showing the presence of C and O in the film. The small signal from Cu is considered to arise from the Li foil that is dissolved in HCl to form the LiCl. The O signal is from the Li_2O formed during heating of the Li-graphene.

structure from nitrogen molecular state may be difficult as the laser energy is not sufficient to fully ionize the N_2 gas. Use of NH_3 may be favorable to incorporate N in the amorphous structure, however, it is corrosive to the regular mechanical pump that is used in the present work. SEM image of LiPON film on LiNiMnO film present on Si is shown in Fig. 5(a) and (b) with EDS presented in Fig. 5(c). The film is smoother than the LiPON film shown in Fig. 4. The signal from P in EDS presented in Fig. 5(c) is over shadowed by the Au peak.

Results of X-ray diffraction, presented in Fig. 2(b), from the

graphene film containing graphene platelets with adsorbed Li from LiCl solution showed the characteristic graphite peaks and a weak peak that is associated with LiC. Thus, the fraction of LiC in the film is small. The surface of the graphene film is not very smooth, as seen in the SEM image in Fig. 6(a) and (b). The presence of O peak in the EDS, presented in Fig. 6(c), may be a result of heating the film to drive out the Cl from the LiCl that is present between the graphene platelets. An external pressure has not been applied to compact the film although a sharp edge is used to smoothen the film. The porous structure at the surface arose from the evolution of Cl from the film.

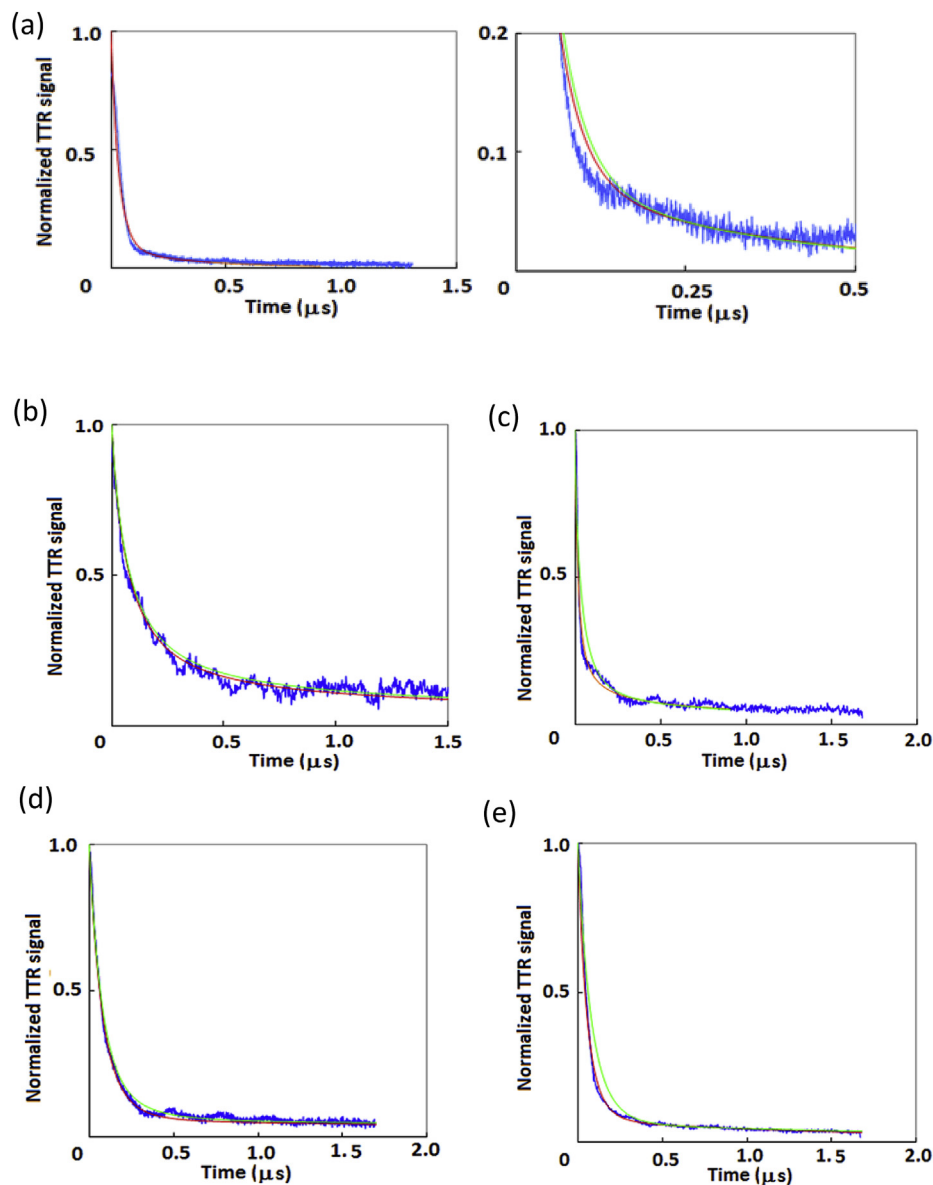


Fig. 7. (a). Normalized TTR signal from (a) the LiNiMnO film on Si. The blue line is the experimental result. The red line is the curve fitted result for values of parameters shown in Table 1. The inset on the right shows the details. The green line is obtained for $K_2 = 30 \text{ W m}^{-1}\text{K}^{-1}$ and $h_{23} = 150 \text{ MWm}^{-2}\text{K}^{-1}$ but with the same values for other parameters. (b). Normalized TTR signal from the LIPON film on Si. The blue line is the experimental result. The red line is the curve fitted result for values of parameters shown in Table 1. The green line is obtained for $K_2 = 6 \text{ W m}^{-1}\text{K}^{-1}$ but with the same values for other parameters. (c). Normalized TTR signal from the LIPON film on LiNiMnO film on Si. The blue line is the experimental result. The red line is the curve fitted result for values of parameters shown in Table 1. The green line is obtained for $K_2 = 5 \text{ W m}^{-1}\text{K}^{-1}$ but with the same values for other parameters. (d). Normalized TTR signal from the Li adsorbed graphene film on Si. The blue line is the experimental result. The red line is the curve fitted result for values of parameters shown in Table 1. The green line is obtained for $K_2 = 30 \text{ W m}^{-1}\text{K}^{-1}$, $h_{12} = h_{23} = 4 \text{ MWm}^{-2}\text{K}^{-1}$ but with the same values for other parameters. (e). Normalized TTR signal from the graphene film on Si. The blue line is the experimental result. The red line is the curve fitted result for values of parameters shown in Table 1. The green line is obtained for $K_2 = 20 \text{ W m}^{-1}\text{K}^{-1}$ and $h_{23} = 1 \text{ MWm}^{-2}\text{K}^{-1}$ but with the same values for other parameters. (For interpretation of the references to colour in this figure legend, the reader is referred to the web version of this article.)

Table 1

Thickness and thermal conductivity of different layers used in the analysis. Thickness of the region 2 or the film is t_2 and thermal conductivity is K_2 . The thickness of region 3 (t_3) of Si substrate and thermal conductivity (K_3) are provided. For the sample with composite layer of LIPON on LiNiMnO, region 2 is LIPON and region 3 is LiNiMnO film as the thermal conductivity of LIPON is low and thermal diffusion is limited to the composite layer. The interface thermal conductance between Au film and region 2 is h_{12} and that between region 2 and region 3 is h_{23} .

Sample	t_2 (μm)	K_2 ($\text{Wm}^{-1}\text{K}^{-1}$)	t_3 (μm)	K_3 ($\text{Wm}^{-1}\text{K}^{-1}$)	h_{12} ($\text{MWm}^{-2}\text{K}^{-1}$)	h_{23} ($\text{MWm}^{-2}\text{K}^{-1}$)
LiNiMnO–Si	0.4	40.0 ± 5	8.0	150	8 ± 1	200 ± 20
LIPON–Si	0.4	7.0 ± 1	8.0	150	8 ± 1	10 ± 2
LIPON–LiNiMnO	0.4	7.0 ± 0.8	0.4	40	50 ± 5	150 ± 15
Graphene–Si	4.0	25.0 ± 2	8.0	150	4 ± 0.5	2 ± 0.5
Li–graphene–Si	4.0	40.0 ± 5	8.0	150	6 ± 1	6.5 ± 1

The sample surface is not expected to be smooth like that of vapor deposited film. However, the presence of graphene platelets with large surface area is helpful in the adsorption of Li from the LiCl solution.

The emphasis of the present work is to determine the thermal conductivity and interface thermal conductance between films in Li-ion batteries. The measurements using TTR are useful to determine the thermal conductivity in the cross-plane direction and the interface thermal conductance. The thermal conductivity of LiNiMnO film of thickness $0.4\ \mu\text{m}$ presented in Table 1, was found to be $K_2 = 40\ \text{W m}^{-1}\text{K}^{-1}$ that is reasonably high. Results presented in Fig. 7(a) illustrate that the thermal conductivity of the film, K_2 , and the interface thermal conductance between the film and the Si substrate, h_{23} , are important parameters. The film is electrically conducting and therefore both electronic and phonon contributions are present. The electronic contribution arises from the presence of Li whereas Ni and Mn oxides are both known to be semiconducting. Therefore, contribution from electronic contribution will be increased in the discharged state as a result of Li incorporation and the opposite happens in the charged state. Phonon contribution is expected to be the dominant term in the thermal conductivity. The interface thermal conductance between Au transducer film and LiNiMnO is found to be $8\ \text{MWm}^{-2}\text{K}^{-1}$ that is a low value. The lower value could be due to several reasons but it is primarily associated with the roughness of the film surface as a result of laser generated particulates [26–28]. The thermal resistance at an interface is strongly dependent on the interface roughness as it reduces the thermal contact [28]. In addition, thermal conductivity is electron mediated in Au while it is predominantly phonon mediated in LiNiMnO. Therefore, electron-phonon coupling is essential which is known to be low in Au [29]. The interface thermal conductance, h_{23} , between LiNiMnO and Si substrate is significantly higher with a value of $200\ \text{MWm}^{-2}\text{K}^{-1}$ so that it is not a barrier to thermal transport. The polished surface of Si, the higher crystallinity of LiNiMnO, and the phonon mode thermal conductivity in both the regions is responsible for the higher value of h_{23} . Thus, the positive electrode material, LiNiMnO, is favorable in terms of thermal energy dissipation.

Results presented in Fig. 7(b) illustrate that the thermal conductivity of LIPON film, K_2 , is an important parameter that determines the TTR signal variation. The thermal conductivity of LIPON film of thickness $0.4\ \mu\text{m}$, shown in Table 1, is significantly lower at $K_2 = 7\ \text{W m}^{-1}\text{K}^{-1}$ and the value of the interface thermal conductance h_{12} between Au and LIPON is also lower at $8\ \text{MWm}^{-2}\text{K}^{-1}$. LIPON is amorphous with short range or local crystalline order between P–O–N and P–O bonds. As a result, the thermal conductivity is not very low as in some amorphous solids such as silica glass [30]. Other estimates [31] of thermal conductivity with a different composition, $\text{Li}_{5.5}\text{PO}_{4.5}\text{N}_{0.6}$, showed a lower value of $K_2 = 1.4\ \text{W m}^{-1}\text{K}^{-1}$ that is much closer to the amorphous limit. The LIPON films deposited in the present work contained much smaller concentration of N in the film that could be another reason for the slightly higher value of K_2 . The value of $h_{23} = 10\ \text{MWm}^{-2}\text{K}^{-1}$ is also low as the amorphous LIPON film and the amorphous surface layers of Si containing N formed during deposition were in contact at the interface. Thus, LIPON film is found to be a barrier to thermal transport across the positive and negative electrodes. Therefore, thermal energy dissipation on both sides of the electrodes must take place through the metal contact layers.

Results presented in Fig. 7(c) illustrate that the thermal conductivity of LIPON is a significant factor in determining the TTR signal variation because the thermal conductivity of LiNiMnO is much higher. The effect of LIPON film in direct contact with LiNiMnO is deduced from the low thermal conductivity of the

LIPON film, $K_2 = 7\ \text{W m}^{-1}\text{K}^{-1}$ and the thermal conductivity of LiNiMnO, $K_3 = 40\ \text{W m}^{-1}\text{K}^{-1}$, presented in Table 1. The thickness t_2 of LIPON is $0.4\ \mu\text{m}$ while that of LiNiMnO or t_3 is $0.4\ \mu\text{m}$. The interface thermal conductance h_{12} between Au and LIPON is $50\ \text{MWm}^{-2}\text{K}^{-1}$ and that of h_{23} between LIPON and LiNiMnO is $150\ \text{MWm}^{-2}\text{K}^{-1}$. The Si substrate was not needed in the simulation of TTR signal, shown in Fig. 7(c), as the thermal diffusion depth was limited to LiNiMnO layer. The slightly higher value of h_{12} is a result of regions of LIPON film with smaller number of particulates and reduced surface roughness. The much higher value of h_{23} is also associated with the better interfacial contact between LIPON and LiNiMnO and the phonon mediated transport in both regions. The net thermal conductance associated with LIPON and LiNiMnO is determined from $1/h_{\text{eff}} = t_2/K_2 + 1/h_{23} + t_3/K_3$ and the resulting value is $h_{\text{eff}} = 18\ \text{MWm}^{-2}\text{K}^{-1}$ which is small although h_{23} and K_3 are reasonably high. These results illustrate that although interface thermal conductance is improved, the lower thermal conductivity of amorphous LIPON is a barrier to thermal transport from positive to negative electrode or vice versa. Thus, the two sides are thermally isolated.

Results presented in Fig. 7(d) illustrate that the thermal conductivity of Li absorbed graphene, K_2 , and the interface thermal conductance with the substrate, h_{23} , are important parameters. Because the thermal conductivity of the film is relatively higher, the value of h_{23} becomes more important in the thermal transport. Similarly, results presented in Fig. 7(e) illustrate that the thermal conductivity of graphene platelets, K_2 , and the interface thermal conductance, h_{23} , are important parameters. The thermal conductivity of graphene film with platelets is known to be high only in the ab plane [32], however, it is low in the C-direction or normal to the ab plane [33]. The thermal conductivity of Li absorbed graphene $K_2 = 40\ \text{W m}^{-1}\text{K}^{-1}$, shown in Table 1, is higher than that of pure graphene film $K_2 = 25\ \text{W m}^{-1}\text{K}^{-1}$ as Li provides a better contact between the platelets. The thermal conductivity of bulk Li is close to $85\ \text{W m}^{-1}\text{K}^{-1}$ and thus much higher than that of graphene in C-direction which is $35\ \text{W m}^{-1}\text{K}^{-1}$. Thermal conductivity of Li-graphene composite film is higher than that of graphene. Therefore, graphene anode exhibits lower heat spreading in the discharged state in the absence of Li. The interface thermal conductance h_{12} between Au and graphene and h_{23} between graphene and Si are both very low, as shown in Table 1. It is also known that the interface thermal conductance between graphene and other media is low [34] but may be improved by functionalization of graphene [34]. However, the roughness of the surface and the poor contact between graphene platelets and Si is responsible for the lower values of h_{12} and h_{23} .

In comparison with other films that are investigated in the present work, graphene platelets show a higher thermal conductivity than the LIPON film but lower than the crystalline LiNiMnO film. The interface thermal conductance of graphene platelets with adsorbed Li is also lower than that of either LIPON or LiNiMnO with Si. Composite films of graphene and Si nano grains that may be used as anodes are also expected to show lower cross-plane thermal conductivity than Si as the interface thermal conductance is lower. The thermal contact is limited between graphene and other films as graphene is inert and only exhibits weak van der Waals bond. The barrier to thermal transport in the films is found to be amorphous LIPON film. Smaller thickness LIPON film is beneficial as long as the film is stable. Alternately, layered composite electrolyte films of LIPON and LiLaTiO_3 (LLT) could improve both ionic conductivity and thermal conductivity and at the same time prevent LLT from chemical instability upon contact with Li ions [35]. The crystalline LLT is expected to have higher thermal conductivity and therefore will improve the value for the composite films above

that of the LIPON film provided the interfacial thermal conductance remains higher.

5. Conclusions

Thin films of LIPON and LiNiMnO used in Li ion batteries have been deposited by LPVD on Si substrate. The graphene film consisting of Li adsorbed graphene platelets or graphene platelets has been deposited on Si substrate from a suspension. The thermal conductivity of the films in the cross-plane was determined by transient thermo reflectance with Au transducer film deposited on the top. The results show that.

1. Amorphous LIPON film has much lower thermal conductivity and forms a barrier to thermal transport in the battery. The interface thermal conductance between Au transducer film and LIPON and between LIPON and Si was found to be lower as a result of the surface roughness and amorphous structure. However, the interface thermal conductance between LIPON and LiNiMnO is much higher.
2. Thermal conductivity of LiNiMnO is higher. The interface thermal conductance between Au and LiNiMnO is lower because of roughness of the film but that between LiNiMnO and Si is higher. Therefore, LiNiMnO is not a thermal barrier.
3. Thermal conductivity of graphene film with Li adsorbed graphene platelets or with pure graphene platelets is also higher but much smaller compared to the in-plane thermal conductivity. The interface thermal conductance between graphene film and the Au transducer or Si is also lower. Thus, thermal transport is limited by the interface thermal resistance.

Acknowledgements

This work was performed in part at the Analytical Instrumentation Facility (AIF), which is supported by the State of North Carolina and the National Science Foundation (award number ECCS-1542015). The AIF is a member of the North Carolina Research Triangle Nanotechnology Network (RTNN), a site in the National Nanotechnology Coordinated Infrastructure (NNCI).

References

- [1] T.M. Bandhauer, S. Garimella, T.F. Fuller, A critical review of thermal issues in Li-ion batteries, *J. Electro. Chem. Soc.* 158 (2011) R1–R25.
- [2] H. Maleki, S.A. Hallaj, J.R. Selman, R.B. Dinwiddie, H. Wang, Thermal properties of lithium-ion battery and components, *J. Electro. Chem. Soc.* 146 (1999) 947–954.
- [3] H. Maleki, J.R. Selman, R.B. Dinwiddie, H. Wang, High thermal conductivity negative electrode material for lithium-ion batteries, *J. Power Sources* 94 (2001) 26–35.
- [4] O.S. Burheim, M.A. Onsrud, J.G. Pharoah, F. Vullum-Bruer, P.J.S. Vie, Thermal conductivity, heat sources and temperature profiles of Li-ion batteries, *ECS Trans.* 58 (2014) 145–171.
- [5] V. Vishwakarma, A. Jain, Measurement of in-plane thermal conductivity and heat capacity of separator in Li-ion cells using a transient DC heating method, *J. Power Sources* 272 (2014) 378–385.
- [6] W. Xu, G. Zhang, B. Li, Effects of lithium insertion on thermal conductivity of silicon nanowires, *Appl. Phys. Lett.* 106 (2015) 173901.
- [7] B. Koo, P. Goli, A.V. Sumant, P.C.D.S. Claro, T. Rajh, C.S. Johnson, A.A. Balandin, E.V. Shevchenko, Toward lithium ion batteries with enhanced thermal conductivity, *ACS Nano* 8 (2014) 7202–7207.
- [8] H. Xia, Y.S. Meng, L. Lu, G. Ceder, Electrochemical properties of non-stoichiometric $\text{LiNi}_{0.5}\text{Mn}_{1.5}\text{O}_{4-\delta}$ thin-film electrodes prepared by pulsed laser deposition, *J. Electrochem. Soc.* 154 (2007) A737–A743.
- [9] J.B. Goodenough, K.-S. Park, The Li-ion rechargeable battery-A perspective, *J. Am. Chem. Soc.* 135 (2013) 1167–1176.
- [10] R. Santhanam, B. Rambabu, Research progress in high voltage spinel $\text{LiNi}_{0.5}\text{Mn}_{1.5}\text{O}_4$ material, *J. Power Sources* 195 (2010) 5442–5451.
- [11] X. Yu, J.B. Bates, G.E. Jellison Jr., F.X. Hart, A stable thin-film electrolyte: lithium phosphorous oxynitride, *J. Electrochem. Soc.* 144 (1997) 524–532.
- [12] J. Hou, Y. Shao, M.W. Ellis, R.B. Moore, B. Yi, Graphene-based electrochemical energy conversion and storage: fuel cells, supercapacitors and lithium ion batteries, *Phys. Chem. Chem. Phys.* 13 (2011) 15384–15402.
- [13] E. Yoo, J. Kim, E. Hosono, H. Zhou, T. Kudo, I. Honma, Large reversible Li storage of graphene nanosheet families for use in rechargeable lithium ion batteries, *Nano Lett.* 8 (2008) 2277–2282.
- [14] M.T. McDowell, S.W. Lee, W.D. Nix, Y. Cui, 25th Anniversary article: understanding the lithiation of silicon and other alloying anodes for lithium-ion batteries, *Adv. Mat.* 25 (2013) 4966–4985.
- [15] H. Zheng, K. Jagannadham, Thermal conductivity and interface thermal conductance in composites of titanium with graphene platelets, *J. Heat. Trans.* 136 (2014) 061301–061319.
- [16] L. Mai, B. Hu, W. Chen, Y. Qi, C. Lao, R. Yang, Y. Dai, Z.L. Wang, Lithiated MoO_3 nanobelts with greatly improved performance for lithium batteries, *Adv. Mater.* 19 (2007) 3712–3716.
- [17] H. Zheng, K. Jagannadham, Interface Thermal conductance between metal films and copper, *Met. Mat. Tran. A* 45A (2014) 2480–2486.
- [18] M.A. Panzer, G. Zhang, D. Mann, X. Hu, E. Pop, H. Dai, K.E. Goodson, *J. Heat. Trans.* 130 (2008) 052401–052409.
- [19] K. Jagannadham, Effect of interfacial interactions on the thermal conductivity and interfacial thermal conductance in tungsten-graphene layered structure, *J. Vac. Sci. Technol.* 32A (2014) 051101–051110.
- [20] K. Jagannadham, Thermal Conductivity, Interface Thermal, Conductance in films of tungsten-tungsten silicide on Si, *IEEE Trans. Electron Devices* 61 (2014) 1950–1955.
- [21] H. Zheng, K. Jagannadham, Transient thermoreflectance from graphene composites with matrix of indium and copper, *APL Adv.* 3 (2013) 032111–032113.
- [22] M. Brown, K. Jagannadham, Thermal conductivity of MWNT–Epoxy composites by transient thermoreflectance, *J. Elect. Mat.* 44 (2015) 2624–2630.
- [23] W.A. Harrison, *Solid State Theory*, Page 263, Dover Publications Inc, New York, 1979.
- [24] J.B. Scarborough, *Numerical Mathematical Analysis*, fourth ed., Oxford University Press, 1958, p. 414.
- [25] J. Leitner, P. Vonka, D. Sedmidubsky, P. Svoboda, Application of Neumann-Kopp rule for the estimation of heat capacity of mixed oxides, *Thermochim. Acta* 497 (2010) 7–13.
- [26] P.E. Hopkins, L.M. Phinney, J.R. Serrano, T.E. Beechem, Effects of surface roughness and oxide layer on the thermal boundary conductance at aluminum/silicon interfaces, in: *Proc. 14th Int. Heat Transfer Conference, IHTC14*, August 8–13, Washington DC 6, 2010, pp. 313–319.
- [27] M. Kazan, A. Bruyant, P. Royer, P. Masri, Thermal conductance of the interfaces between the III-nitride materials and their substrates: effects of intrinsic material properties and interface conditions, *Surf. Sci. Rep.* 65 (2010) 111–127.
- [28] B.N.J. Persson, Thermal interface resistance: cross-over from nanoscale to macroscale, *J. Phys. Condens. Matter* 26 (2014) 015009–015011.
- [29] A. Birch, W.R.G. Kemp, P.G. Klemens, R.J. Tainsh, Lattice thermal conductivity of some gold alloys, *Aust. J. Phys.* 12 (1959) 455–465.
- [30] D.G. Cahill, R.O. Pohl, Thermal conductivity of amorphous solids above the plateau, *Phys. Rev. B* 35 (1987) 4067–4073.
- [31] F. Xu, C. Fretigny, D. Fournier, L. Belliard, S. Vincent, B. Perrin, S. Martin, C. Secouard, J.-Y. Duquesne, Lateral heat diffusion investigation of a layered structure: applications to the complete thermal characterization of lithium phosphorous oxynitride film 113, 2013, pp. 244304–244316.
- [32] A.A. Balandin, S. Ghosh, W. Bao, I. Calizo, D. Teweldebrahn, F. Miao, C.N. Laue, Superior thermal conductivity of single layer graphene, *Nano Lett.* 8 (2008) 902–907.
- [33] P.G. Klemens, Theory of thermal conduction in thin ceramic thin films, *Int. J. Thermophys.* 22 (2001) 265–275.
- [34] E. Hopkins, M. Baraket, E.V. Barnat, T.E. Beechem, S.P. Kearney, J.C. Duda, J.T. Robinson, G.S. Walton, Manipulating thermal conductance at metal-graphene contacts via chemical functionalization, *Nano Lett.* 12 (2012) 90–95.
- [35] C.L. Li, B. Zhang, Z.W. Fu, Physical and electrochemical characterization of amorphous lithium lanthanum titanate solid electrolyte thin film fabricated by e-beam evaporation, *Thin Solid Films* 515 (2006) 1886–1892.